ITERATIVE REFRACTION-CORRECTION METHOD ON MVS-SfM FOR SHALLOW STREAM BATHYMETRY

A. M. Lingua [1], P. Maschio [1], A. Spadaro [1, *], P. Vezza [1], G. Negro [1]

[1] Department of Environment Land and Infrastructure Engineering (DIATI), Torino, Italy –
(andrea.lingua, paolo.maschio, alessandra.spadaro, paolo.vezza, giovanni.negro)@polito.it

KEY WORDS: UAV/UAS, Structure-from-Motion, Bathymetry, Multi-View Stereo Photogrammetry, Refraction correction.

ABSTRACT:

Extracting accurate bathymetric information from clear, shallow waters in complex riverine environments can be challenging, but it is crucial for many applications, such as hydraulic modeling, ecological monitoring, and sediment transport analysis. Multi-view stereo photogrammetry (MVS-SfM) has emerged as a promising technique for acquiring high-resolution bathymetric data from aerial imagery. However, the accuracy of MVS-SfM can be affected by various factors, including water refraction, which can distort the depth measurements. In this study, iterative Dietrich's refraction-correction method is tested for extracting bathymetry from MVS-SfM in a complex riverine environment. Moreover, we proposed a workflow for applying the method using raster data files, which can be more readily available than point clouds. It also compared the obtained results with previous applications and evaluated them using statistical indices and ratios. For this case study, the multicamera refraction method produces bathymetric datasets with accuracies of ~0.019% of the flying height and precisions of ~0.07% of the flying height. This study contributes to increased confidence in exploiting aerial imagery for bathymetric mapping in photogrammetric procedures under field conditions and can facilitate the management and conservation of clear water systems.

1. INTRODUCTION

Stream bathymetry, measuring water depth and bottom topography, is a critical variable in fluvial geomorphology, alongside variables like width, slope, and velocity, for characterizing the wide range of physical and biological parameters in river systems (Dietrich, 2016).

In larger rivers, traditional bathymetric survey techniques such as sonar, airborne LiDAR (Light Detection And Ranging) sensors, or Acoustic Doppler Current Profiler are proven effective for bathymetry measurement (Klemas, 2011; Leon et al., 2015; Panagou et al., 2020). However, these instruments can be impractical or costly in smaller, shallower streams with depths of less than 2 m. To collect high-resolution bathymetric data, we are forced to use traditional survey techniques such as total station or real-time kinematic global positioning systems (RTK-GPS), which are often limited in spatial scale and time-consuming (Bangen et al., 2014).

As a result of the growing application of Structure-from-Motion (SfM) photogrammetry, which involves a series of overlapping photographs from different angles, the improvement of computational power and specialized software that use computer vision algorithms to generate a three-dimensional model (Carrivick et al., 2016), and the rapid expansion of Uninhabited Aircraft Vehicle (UAV), another method for collecting high-resolution bathymetric data via optical remote sensing has emerged. However, using the photogrammetric technique to analyze underwater environments requires certain conditions, e.g., clear, and calm water surfaces, visibility by means of turbidity, and surface textures of underwater areas (Mandlburger, 2019). But the main restriction is that the in-water measurements are affected by refraction, the bending of the light as it passes the water/air interface; this causes in-water measurements to appear shallower, referred to as the apparent depth, compared to the actual depth. (Dietrich, 2016; Mandlburger, 2019). To improve the reconstruction precision, J. Dietrich (2016) proposed an iterative approach considering camera parameters and viewing angles (in their refraction correction) that calculates a series of refraction correction equations for every point/camera combination in an SfM point cloud.

Overall, this paper aims to a) test the iterative Dietrich's refraction-correction method for extracting shallow stream bathymetry from multi-view stereo photogrammetry (MVS-SfM) in a complex riverine environment, b) propose a workflow for applying the method using raster data files (orthophoto and Digital Elevation Model (DEM)) instead of a point cloud, c) compare the obtained results, including statistical indices and ratios with previous applications d) increase confidence in exploiting aerial imagery of clear, shallow waters for bathymetric reconstruction in photogrammetric procedures under field conditions.

1.1 Previews application

The results of the refraction correction algorithm will be compared with those of the two case studies analyzed by Dietrich (2016). A controlled area was a pool with shallow water approximately 15 cm and 1.2 m in diameter, filled with coarse gravel; the photosets (51 photographs) were collected with a DJI Phantom 3 Advanced (P3A) quadcopter at 8m and 12 m above ground level (a.g.l.) and off-nadir ~20° angle; the point cloud was subsampled with a point spacing of 0.01 m, and 4.960 refraction corrected points were analyzed by Dietrich's algorithm.

Fieldwork was carried out in ~ 250m reach of the White River in Vermont, with a maximum depth of ~1.5m and bed sediment ranging from fine sand to cobbles. Two sets of images were collected, one in October 2015 and another in June 2016. The photographs for the October flight (190 photographs) were taken with a DJI Inspire 1 at 40 and 60m a.g.l., while the June images (220 photographs) were taken with a P3A quadcopter at 60 and 80m a.g.l. Using a point spacing of 0.30m, 93,600 and 121,300 points from October and June, respectively, were corrected by refraction. The accuracy of the correction, the relative accuracy and the precision ratio were used to compare the results of different applications.

* Corresponding author

1.2 Case study

The application area is a ~ 220 m reach of the Chisone River in Val Troncea, Piedmont, Italy (Figure 1). The ellipsoidal height ranges between 1792 and 1805 meters, and the water depth ranges from a few centimeters to 2 meters near the upstream weir. The survey was carried out by the DIATI Department of Politecnico di Torino in collaboration with the Ente di Gestione delle Aree Protette del Parco Alpi Cozie in October 2021.

The flight was conducted in manual mode due to the complex conformation of the survey area, with narrow valleys and dense vegetation, keeping an in-strip overlap of 80% and a between-strips overlap of 60%. The images were taken with a DJI Phantom 4 Pro RTK quadcopter (FC6310R Camera Model), with a focal length of 8.8 mm, 5472x3648 resolution and 2.41x2.41 µm of pixel size. The SfM photographs totaled 216; the flight height was ~63 m a.g.l., with a Ground Simple Distance of 1.54 cm/pix. A rapid-static GNSS survey was conducted to establish GCPs, materialized with 30 cm square checker-board targets and natural points. In addition, 66 streambed points, including three cross-sections, were also surveyed for validation purposes.

The dataset was processed in Agisoft Metashape Pro (version 1.7.3), a commercial software incorporating Structure-from-Motion (Westoby et al., 2012) and MVS algorithms.

Using the tie point, the software aligns the aerial images creating a sparse dense cloud; then calculates a dense point cloud (with MVS) and creates three-dimensional models, serving as the base for the DEMs and orthophotos. The alignment, georeferencing, and dense cloud reconstruction were processed with 'high quality'. The georeferencing accuracies are reported in Table 1. DEM has a resolution of 3 cm/pix and a point density of 0.106 point/cm^2. The orthophoto reconstruction parameters were 'mosaic' *blending mode*, and the *surface reconstruction* was based on DEM. Other settings for the processing steps in Metashape are listed in Table 2.

	X error [m]	Y error [m]	Z error [m]	XY error [m]	Total error [m]
GCPs	0.0108	0.0137	0.0100	0.0175	0.0201
Check Points	0.0274	0.0110	0.0357	0.0313	0.0475

Table 1. GCPs and Check Points georeferencing errors.

Processing step	Setting	Value
Alignment	Accuracy	High
	Reset current alignment	✓
	Reference preselection	Source
	Generic preselction	x
	Key point limit	40000
	Tie point limit	4000
	Adaptive camera model fitting	x
Optimization parameters	Parameters	f, b1, b2, cx, cy, k1-k3, p1, p2
	Adaptive camera model fitting	x
Depth Maps	Quality	High
	Filtering mode	Moderate
Dense point cloud	Quality	High
	Depth filtering	Moderate
	Reuse depth maps	x
	Calculate point colors	✓
DEM	Source data	Dense cloud
	Interpolation	Enabled
	Point classes	All
Orthomosaic	Use custom region Resolution (m)	x
	Surface	DEM
	Blending mode	Mosaic
	Hole filling	✓
	Enable ghosting filter	x

Table 2. Settings and values in Agisoft Metashape used throughout this study.

2. METHODS

2.1 Theoretical principles

The use of photogrammetry provides a technique to measure stream bathymetry directly in clear water systems. However, the main restriction is that the in-water measurements are affected by refraction and the light's bending as it passes the water/air interface (Woodget et al., 2015; Dietrich, 2016). A diagram of the refraction trigonometry of a single measurement point/camera combination is shown in Figure 2, and the variable definitions are given in Table 3.

This causes in-water measurements to appear shallower, referred to as the apparent depth (h_a), compared to the actual depth (h). Snell's Law governs the refraction of light between two different media, air and water in this case:

$$n_1 \cdot \sin i = n_2 \cdot \sin r, \qquad (1)$$

where

n_1 = refractive index of fresh water
n_2 = refractive index of air
i = angle of incidence from the stream bed to the air/water interface (1.337) (Harvey et al., 1998)
r = angle of refraction from the air/water interface to the camera (1.0)

Although in traditional stereophotogrammetry, the point is observed from two overlapping images, complicating the direct application of Snell's Law, in the MVS-SfM dataset, we add multiple views (3-20) for a single point, significantly complicating the refraction correction procedure. Each camera is viewing the streambed from a distinct angle and, according to Snell's Law, should produce different angles of

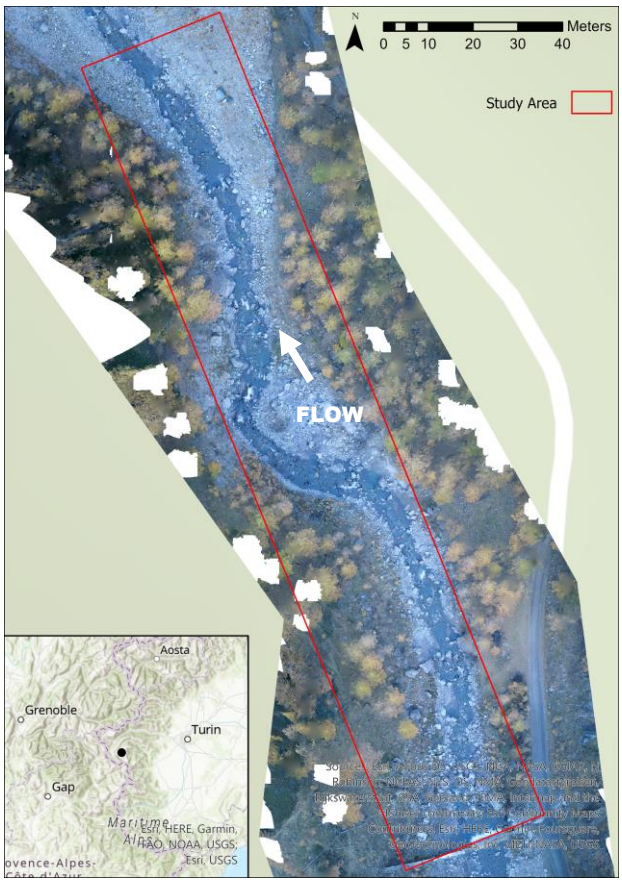

Figure 1. Orthophoto of the application area, Chisone River in Val Troncea, Piedmont, Italy.

incidence and refraction (angle *i* and *r*) and, therefore different apparent depths (h_a), which would create a noise point cloud.
For these reasons, a simplified version of Snell's Law is used with the small-angle approximation substitution proposed by Woodget et al. (2015) specifically for nadir SfM imagery. For angles of less than 10° ($\theta = r \parallel i$), the $sin\theta \cong tan\theta$ and considering the trigonometry of the refraction angles in Figure 2:

$$\sin i \cong \tan i = \frac{x}{h} \quad , \qquad \sin r \cong \tan r = \frac{x}{h_a} \qquad (2)$$

and Equation 1 simplifies to Equation 3:

$$h = 1.337 \cdot h_a \quad , \qquad (3)$$

where *r* and *i* are the angles of incidence and refraction, *x* is the distance from the water/air interface to the point, *h* is the actual depth, and h_a is the apparent depth.
Based on these theoretical principles, J. Dietrich (2016) proposed a multi-camera refraction correction algorithm that calculates a series of refraction correction equations for every point/camera combination in an SfM point cloud.
For each point in the submerged portion of the SfM point cloud, Dietrich's iterative method calculates the refraction correction equations and iterates through all the possible point-camera combinations. It can be thought of as a series of steps:

1. Test the visibility of points from all the cameras that were used in the MVS-SfM reconstruction.
2. Calculate the approximate ground coordinates for the corners of the camera's instantaneous field of view (IFOV) for each camera in the dataset, based on the exterior orientation parameters and the camera's internal parameters.
3. Calculate the angle of refraction *r* for the point cloud points that fall within the calculated IFOV (Equation 4):

$$r = \tan^{-1}\frac{D}{dH}, \qquad (4)$$

   where *D* is the Euclidean distance between the camera and the target point and *dH* is the height difference between the camera and the target point.
4. Calculate the water surface elevations for each visible point.
5. Calculate the angle of incidence *i* (Equation 5), the distance from the SfM point to the air/water interface point *x* (Equation 6), the correct depth of the point that is taken as the mean of all h values *h* (Equation 7) (Butler et al., 2002) and the correct elevation Z_p (Equation 8):

$$i = \sin^{-1}\left(\frac{n_2}{n_1}\cdot \sin r\right), \qquad (5)$$

$$x = h_a \cdot \tan r \quad , \qquad (6)$$

$$h = \frac{x}{\tan i} \quad , \qquad (7)$$

$$Z_p = WS_z - h \quad , \qquad (8)$$

Each in-water point is corrected by the refraction and a high-resolution bathymetric reconstruction is possible using the correct elevation Z_p.

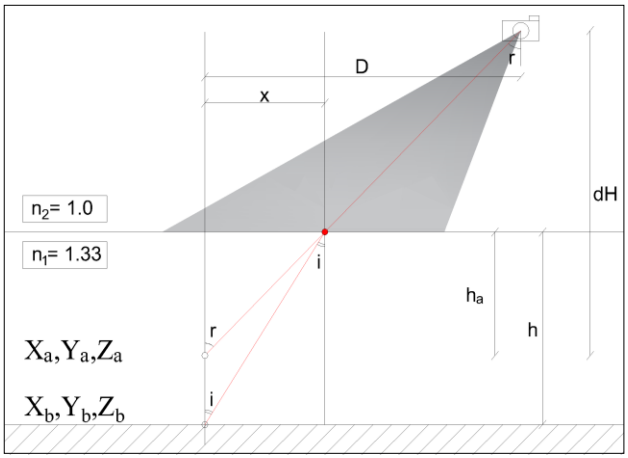

Figure 2. Diagram of the refraction trigonometry.

Variable	Description
X_a,Y_a,Z_a	apparent coordinates of the Structure-from-Motion (SfM) point
X_b,Y_b,Z_b	true coordinates of the point
D	Euclidean distance to the SfM point from the camera
dh	flying height above SfM point
r	angle of refraction
i	angle of incidence
x	distance from the SfM point to the air/water interface point
h_a	apparent depth to the SfM point
h	true depth of point
n_1	refractive index of fresh water (1.337)
n_2	refractive index of air (1.0)

Table 3. Variable definitions in Figure 2 and throughout the text.

2.2 Prerequisite of method's application

For proper application of the method, some conditions are required. Regarding the site condition, clear water is the most crucial factor for accurate depth measurement using SfM. A high level of sediment, which leads to turbid or brown water, can impede the effectiveness of measurement (Mandlburger, 2019). Minimal surface waves are essential. Wind-generated or hydraulic waves can introduce "noise" into the point cloud (Dietrich, 2016), causing inaccuracies and errors in the final output. Cloudy or foggy weather conditions can result in numerous reflections on the water surface, hindering precise measurements. Regarding image acquisition, they should be collected at low-oblique angles (~20° off-nadir) in convergent, overlapping patterns. A polarizing filter, adjusted to reduce glare, will help the camera see through the water column to the bottom. Minimizing shadows from banks or vegetation is advisable as much as possible; it is useful to keep the sun behind the sensor. In addition to the ground control points, which are critical for any SfM collection, in-water validation points at different depths are required for error checking and validation.

2.3 Workflow and software

For the correction process, a custom Python script written by Dietrich (2016) is used and available from a GitHub repository (http://github.com/geojames/py_sfm_depth). The script input files are three, and they must be comma-delimited files (*.csv).
The *Dense Cloud File* containing the point cloud is to be corrected. For each point are known the coordinates (*x* and *y*),

the bathymetric elevation of the point measured by the SfM dataset (*sfm_z*) and the water surface elevation (*w_surf*). The header line of the file must necessarily be *x, y, sfm_z, w_surf.*

Cameras File, the export file of the positions (*x,y,z*) in the same reference system as the points and orientations (*pitch, roll, yaw*) of the cameras in which 0° is nadiral, horizontal, and heading northward. The header line of the file must necessarily be *x,y,z, pitch, roll, yaw*.

Sensor File contains the focal length of the camera (focal) in millimeters and the physical dimensions of the sensor also in millimeters (*sensor_x and sensor_y*). The header line of the file must necessarily be *focal, sensor_x, sensor_y*.

In the output file, also a comma-delimited file (*.csv), for each refraction corrected point are reported the coordinates (*x* and *y*), the SfM measured bathymetric elevation (*sfm_z*), the water surface elevation (*w_surf*) and the apparent depth to be corrected (h_a), the depth (*h_avg*) and the elevation (*corElev_avg*) corrected by the algorithm.

The header line of the output file is *x,y,sfm_z,w_sup h_a,h_avg, corElev_avg*. In Figure 3, a summary schema is reported.

Overall, water surface elevation is the most critical evaluation since camera positions and orientations are easily exportable by any commercial SfM software, as are camera sensor parameters (focal length, sensor size).

For the White River site (paragraph 1.1.), Dietrich (2016) defined the water surface using global positioning system (GPS) points along the water's edge and supplemented them with additional points digitized from the water's edge visible in the SfM point cloud. Instead, for the Chisone River application, the water surface is generated using a Kriging interpolation surface, starting from the orthophoto and Digital Elevation Model (DEM) data exported from Metashape, both with a resolution of 5 cm/pix. The aim was to test a less time-consuming and costly method.

The steps explained below are summarized in Figure 4; the procedure was conducted in Agisoft ArcMap (version 10.8), a commercial software. First, I create a point shapefile to digitalize the water's edge (119 points) visible in the orthophoto (red points in Figure 5). It is recommended to place them as close as possible in elevation to the water surface, in pairs between banks. It is good practice to place a greater number of points where there are abrupt changes in slope and a smaller number where the slope is constant for long stretches.

The elevation was then associated with each point, based on the DEM. The water surface (Figure 5) was generated using Kriging interpolation (*Arctoolbox/Kriging* in ArcMap), using the digitalized water's edge points as *import point feature*, the DEM elevation as *Z value field*, Ordinary *Kriging Method* and

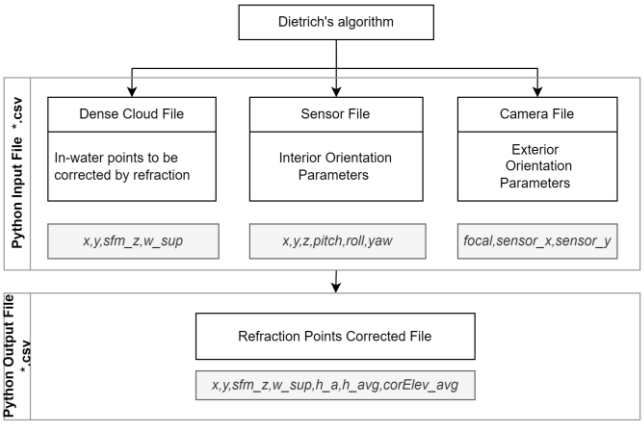

Figure 3. Python script input and output files.

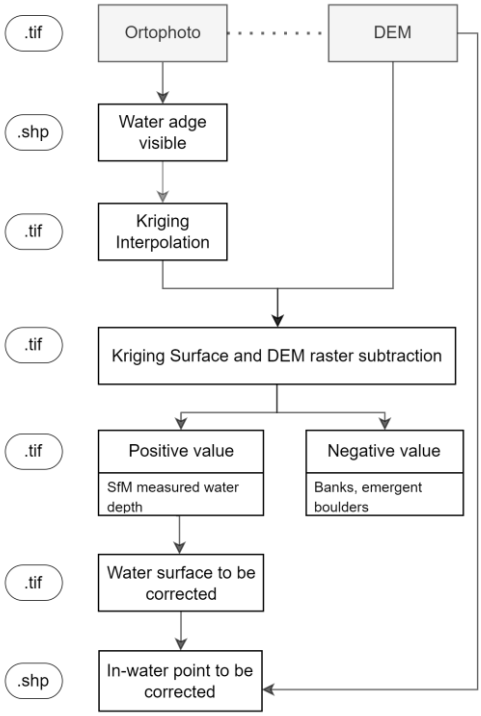

Figure 4. Workflow of water surface extraction.

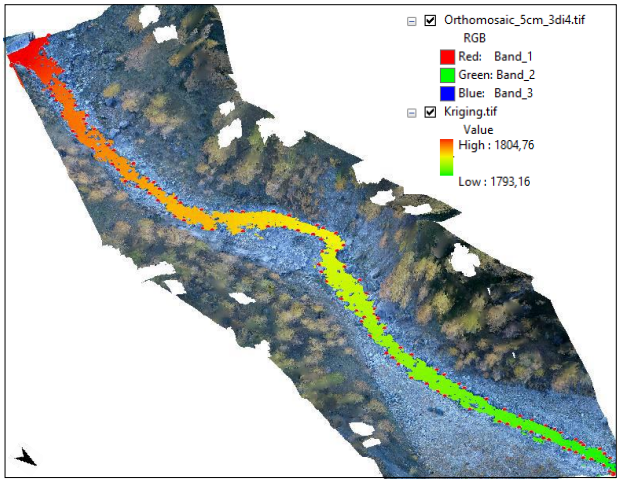

Figure 5. Water's edge points and kriging interpolation surface.

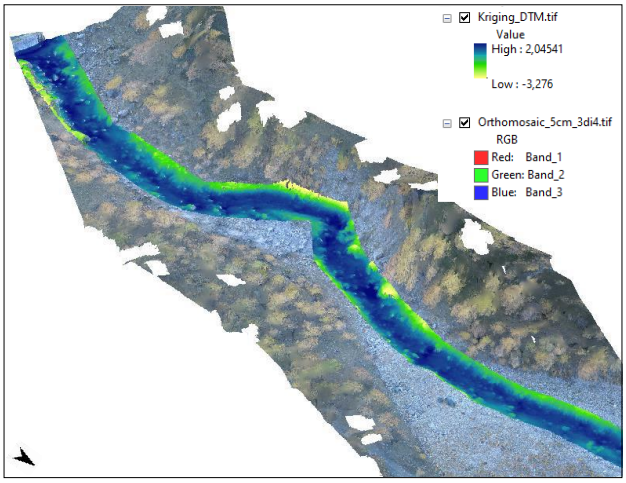

Figure 6. Subtraction between Kriging Surface and DEM raster.

Spherical *Semivariogram model*. It is necessary to set the output cell size of the raster the same as the orthophoto and DEM, to facilitate subsequent steps.
To determine the in-water point to be corrected by Dietrich's algorithm, a raster subtraction between the Kriging surface and the DEM was done (*Raster calculation tool* in ArcMap).
A new raster file has been created with values ranging from -3,20 m to +2,04 m (Figure 6); positive values (water depth) represent the flow points (blue areas in Figure 6) while negative ones are banks or emergent boulders (green areas in Figure 6). After extracting those positive values, the surface to be corrected was generated.
A point cloud is required for the Python script implementation, specifically for the *Dense Cloud File*. The raster transformation into a point shapefile was done considering the center of the pixel (one point every 5 cm). Finally, each of these points was assigned planimetric coordinates (*x* e *y*), the bathymetric elevation from the DEM (*sfm_z*) and the water surface elevation from the interpolated Kriging surface (*w_surf*).

3. RESULTS AND DISCUSSION

In the Chisone River, Dietrich's algorithm was used to correct 460.924 points, one for each 5 cm, according to the orthophoto and DEM cell size. Figure 7 shows 1) the spatial distributions of the elevation error of the 66 GPS-measured validation points, calculated as the difference between GPS-measured data and corrected SfM data: positive errors (red squares in Figure 7) indicate that the corrected SfM elevation is above the GPS measured elevation, therefore under-predicting the depth, while negative errors (purple circles in Figure 7) indicate the opposite ones and therefore over-predicting the depth; and 2) the bathymetric mapping reconstruction generated by the refraction-corrected points, obtained by converting a point shapefile to raster file. The distribution errors do not show any large-scale systematic ones; areas with more errors can be related to noisier original point clouds due to waves o shadows. Table 4 compares the overall error statistics and some other parameters of the Chisone River analysis with Dietrich's applications (pool and White River). The case study dataset has a small positive bias in the Mean Elevation Error (0.004m), as shown in the histograms in Figure 8. The Mean Square Error is 0.01 slightly higher compared to the application of the White River in 2015 (0.006). The Mean Absolute Error is 0.07 and the Root Mean Square Error (RMSE) is 0.01. The Minimum Error is -0.26 m and the Maximum one is 0.33 m. To analyse the data on a small-scale, Figure 9 displays the resulting profiles from R_2 and R_3 sections (Figure 7). A grey line represents the GPS-measured profiles, while a red line indicates the SfM profiles; the green line represents the SfM refraction-corrected profiles. A preliminary qualitative analysis shows that the algorithm has produced excellent results in correcting the depth while properly maintaining the bathymetric trend.

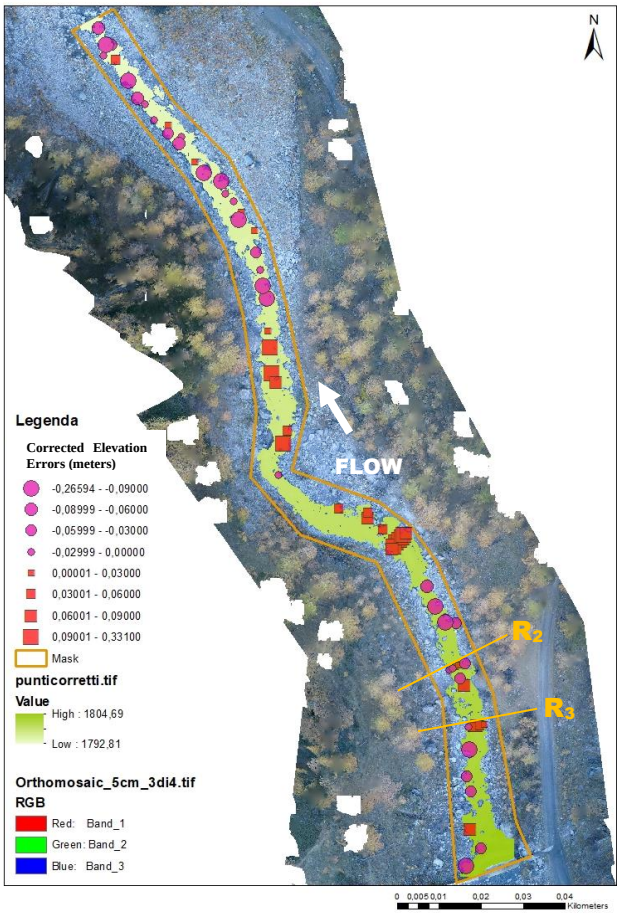

Figure 7. Spatial distributions of the elevation error of GPS-measured validation points.

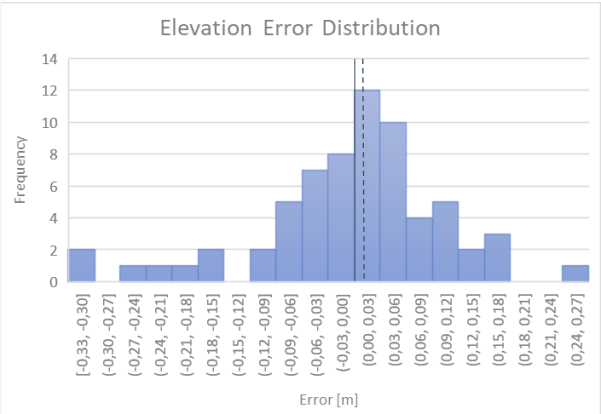

Figure 8. Histogram of elevation error distribution.

	Subsampled in-water points [cm]	Points number [-]	Flight Height Range [m]	Maximum depth [m]	Mean Error [m]	Mean Square Error [m]	Mean Absolute Error [m]	RMSE [m]	Minimum Error [m]	Maximum Error [m]	Relative Accuracy Ratio	Relative Precision Ratio
Chisone River	5	460.924	60-70	2.00 m	0.004	0.011	0.075	0.106	-0.266	0.331	1:5336	1:1260
Pool	1	4.960	10-12	0.173	0.0017	0.0000	0.0032	0.0040	-0.0114	0.0131	1:5882	1:2778
White River (2015)	30	93.600	40-60	1.80	-0,011	0.006	0.056	0.077	-0.262	0.291	1:4545	1:649
White River (2016)	30	121.300	60-80	1.80	0.014	0.003	0.039	0.061	-0.112	0.381	1:5000	1:1186

Table 4. Comparison table of statistical errors and analysis parameters.

Figure 9. R_2-R_3 section: GPS-measured profile (grey line), SfM-measured profile (red line) and SfM refraction-corrected profile (green line).

The profiles of the corrected-refraction data closely approximate and in some cases exactly match, those of the GPS-measured data. In the R_2 section (Figure 9, left part), the maximum error of 10 cm was reduced to 5 cm, and the minimum error of 2.4 cm was eliminated. For four out of eight points, the error was reduced to zero, while for the remaining points, it is around 2 cm. In the R_3 section (Figure 9, right part), the maximum of 15 cm was reduced to 3 cm, and the error is around 3 cm for the other points. Overall the qualitative analysis and error statistics indicate that the refraction correction algorithm produces correct altitudes, relative accuracy and precision ratios (James and Robson, 2012) are calculated to quantify the data errors at different spatial scales; these ratios effectively compare the accuracy of the results between the different applications (Table 4). In the Chisone River application, the accuracy ratio is 1:5336 (0,019%) and the precision ratio is 1:1260 (0,079%), considering a flight height of ~63 m. Compared with the White River application, in which the accuracy ratios for October were 1:4545 (0.022% flying height) and June 1:5000 (0.02%), and the precision ratios for October were 1:649 (0,15%) and June 1:1186 (0.08%), the results demonstrate that the MVS-SfM corrected data has significantly improved accuracy and precision.

Figure 10 are also shown the scatter plots of corrected elevation and depth; the coefficient of determination R^2, which expresses the regression function's quality to approximate the mean elevation and depth difference, is 0,99 and 0,94, respectively; the regression lines also demonstrate that there is no correlation between the errors increasing with rising depths.

We can state that Dietrich's method has produced accuracies comparable to those achieved in the White River applications, and also in a complex river environments application, using orthophoto and DEM as input data. The level of accuracy demonstrated should be sufficient for many river system applications.

The advantage is therefore the possibility of application even without having a 3D model available by following the workflow studied for this case study. Similarly, the water surface extraction can be performed without using global positioning system (GPS) points along the water's edge. However, sources of error encountered during refraction correction include (but are not limited to) georeferencing errors, point cloud noise, errors on the water surface, as well as limitations imposed by the use of SfM data. One limitation could therefore be the risk of not having control over the errors associated with the data generation process, i.e., the orthophoto and DEM. It has also been demonstrated that this method can generate an accurate bathymetric map even in complex environments with steeper river slopes and fragmented flow directions, with higher resolution compared to previous applications in river environments (one point per 5 cm instead of 30 cm).

Note that the point spacing should ultimately be defined by the site and the research question that the data are being used to answer, and in this case also by the resolution of the raster data.

Future developments concern the automation of the process, both regarding the extraction of the water surface and the generation and setting of the three input files (*Dense Cloud*, *Camera*, and *Sensor files*) through the programming of scripts using the ArcGIS API for Python and integrated them into Jupyter Notebook in ArcGIS Enterprise. Optimizing the Python code regarding debugging and problem identification is also fundamental to making it more user-friendly.

This research, like others (Westaway et al., 2001; Butler et al., 2002) used the mean of the calculated depth values (h),

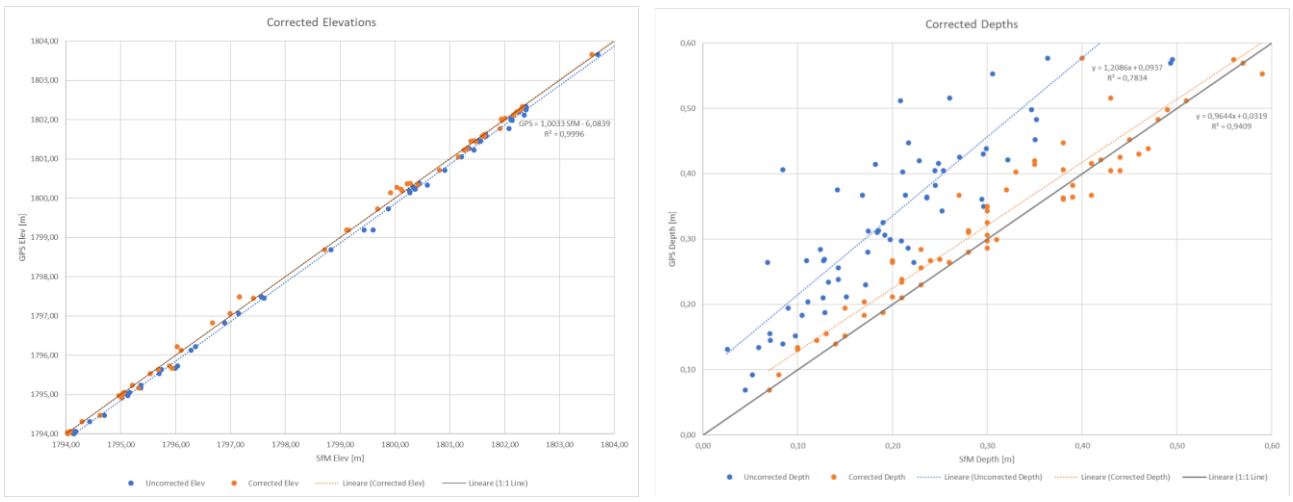

Figure 10. Scatter plots of corrected depths and elevations.

resulting in acceptable accuracy. Further research will explore additional statistical measures, such as median or percentile ranks, for the distributions of h values at each point. The aim is to investigate whether these measures offer any enhancements in terms of accuracy or precision. An alternative to these fundamental statistical measures may be a complex weighted average method that considers variables such as the angles (*r* and *i*) and camera lens parameters. (Dietrich, 2016).

4. CONCLUSION

This study tested the effectiveness of the iterative Dietrich's refraction-correction method for extracting shallow stream bathymetry from multi-view stereo photogrammetry (MVS-SfM) in a complex riverine environment. The proposed workflow using raster data files (orthophoto and Digital Elevation Model) instead of a point cloud showed promising results in accurately estimating bathymetry in clear, shallow waters, with mean errors of 0,019% of the flying height. Comparisons with previous applications and statistical analyses demonstrated that the iterative correction method improved the accuracy of the MVS-SfM data. Using raster data files in the workflow provided a faster and more efficient alternative to point cloud processing while maintaining high accuracy. This study also contributes to increased confidence in exploiting aerial imagery for bathymetric reconstruction in photogrammetric procedures under field conditions. The results showed that photogrammetry could be a cost-effective and efficient method for bathymetry mapping in rivers and streams, especially in areas where traditional bathymetric survey methods are limited or not feasible. Future research should focus on exploring the potential of MVS-SfM and the iterative correction method in other types of water bodies with different characteristics and environmental conditions. Additionally, photogrammetric techniques' accuracy could be improved by exploring other statistical measures for the distributions of *h* values at each point. Overall, the results of this study demonstrate the potential of photogrammetry to improve our understanding of river and stream morphology and dynamics.

ACKNOWLEDGMENTS

The authors thank the Ente di Gestione dei Parchi delle Alpi Cozie (Dr Bruno Aimone, Dr Barbara Rizzioli, and Dr Alba Meirone) for funding the research and Andrea Comè and Beatrice Pinna for collaborating in the activities.

REFERENCES

Dietrich, J.T., 2016: Bathymetric Structure-from-Motion: extracting shallow stream bathymetry from multi-view stereo photogrammetry. *Earth Surface Processes and Landforms*. doi.org/10.1002/esp.4060.

Klemas V., 2011: Beach Profiling and LIDAR Bathymetry: An Overview with Case Studies. *J. of Coastal Research*. doi.org/10.2112/JCOASTRES-D-11-00017.1

Leon J., Roelfsema C.M., Saunders M.I., Phinn S.R., 2015: Measuring coral reef terrain roughness using 'Structure-from-Motion' close-range photogrammetry. *Geomorphology in the Geocomputing Landscape: GIS, DEMs, Spatial Analysis and Statistics.* doi.org/10.1016/j.geomorph.2015.01.030

Panagou T., Oikonomou E., Hasiotis T., Velegrakis A.F., 2020: Shallow Water Bathymetry Derived from Green Wavelength Terrestrial Laser Scanner. *Marine Geodesy 1–21*. doi.org/10.1080/ 01490419.2020.1737602

Bangen S.G., Wheaton J.M., Bouwes N., Bouwes B., Jordan C., 2014: A methodological intercomparison of topographic survey techniques for characterizing wadeable streams and rivers. *Geomorphology* doi.org/10.1016/j.geomorph.2013.10.010.

Carrivick J.L., Smith M.W., Quincey D.J., 2016: Structure from Motion in the Geosciences. *John Wiley & Sons Ltd*. doi.org/10. 1002/9781118895818

Mandlburger G., 2019: Through-Water Dense Image Matching for Shallow Water Bathymetry. *Photogrammetric Engineering and Remote Sensing*. doi.org/10.14358/PERS.85.6.445

Westoby M., Brasington J., Glasser N., Hambrey M., Reynolds J., 2012: Structure-from-motion photogrammetry: A low-cost, effective tool for geoscience applications. *Geomorphology* 179:300–314. doi.org/10.1016/j.geomorph.2012.08.021

Harvey A.H., Gallagher J.S., Sengers J.M.H.L., 1998: Revised formulation for the refractive index of water and steam as a function of wavelength, temperature and density. *Journal of Physical and Chemical Reference*, Data 27, 761–774. doi.org/10.1063/1.556029.

Woodget, A.S., Carbonneau P.E., Visser F., Maddock I.P., 2015: Quantifying submerged fluvial topography using hyperspatial resolution UAS imagery and structure from motion photogrammetry. *Earth Surface Processes and Landforms*, 40, 47–64. doi.org/10.1002/esp.3613.

Butler J., Lane S., Chandler J., Porfiri E., 2002: Through-water close range digital photogrammetry in flume and field environments. *The Photogrammetric Record* 17: 419–439. doi.org/10.1111/0031-868X.00196.

Dietrich JT (2016) py_sfm_depth homepage. http://github.com/geojames/py_sfm_depth

Agisoft, 2019: Agisoft Metashape User Manual: Professional Edition, Version 1.5. https://www.agisoft.com/pdf/metashape-pro_1_5_ en.pdf

James M.R., Robson S., 2012: Straightforward reconstruction of 3D surfaces and topography with a camera: accuracy and geoscience application. *Journal of Geophysical Research*: *Earth Surface* 117. doi.org/:10.1029/2011JF002289.F03017

Westaway R.M., Lane S.N., Hicks D.M., 2001: Remote sensing of clearwater, shallow, gravel-bed rivers using digital photogrammetry. *Photogrammetric Engineering and Remote Sensing* 67: 1271–1282.

Butler J, Lane S, Chandler J, Porfiri E., 2002: Through-water close range digital photogrammetry in flume and field environments. *The Photogrammetric Record* 17: 419–439. doi.org/:10.1111/0031-868X.00196